Electronic Supplementary Material (ESI) for Journal of Materials Chemistry A.

Hybrid Implanted Hybrid hollow nanocubes electrocatalyst facilitates efficient hydrogen evolution activity

Fuxin Wang,[a†] Lei Hu,[a†] Ran Liu,[d] Hao Yang,[a] Tuzhi Xiong,[b] Yanchao Mao,[c] M.-Sadeeq (Jie Tang) Balogun,*[b] Gangfeng Ouyang,*[a] and Yexiang Tong*[a]

[a]MOE of the Key Laboratory of Bioinorganic and Synthetic Chemistry, The Key Lab of Low-Carbon Chemistry & Energy Conservation of Guangdong Province, School of Chemistry, Sun Yat-sen University, Guangzhou 510275, People's Republic of China.

[b]College of Materials Science and Engineering, Hunan University, Changsha 410082, Hunan, People's Republic of China.

[c]MOE Key Laboratory of Materials Physics, School of Physics and Engineering, Zhengzhou University, Zhengzhou 450001, China

[d]Division of Engineering Science, Faculty of Applied Science & Engineering, University of Toronto, St. George (Downtown Toronto) Campus, 27 King's College Cir, M5S, Toronto, ON

*****Corresponding Author**:**

M.-Sadeeq (Jie Tang) Balogun; E-mail: balogun@hnu.edu.cn

Gangfeng Ouyang; E-mail: cesoygf@mail.sysu.edu.cn

Yexiang Tong; E-mail: chedhx@mail.sysu.edu.cn

Experimental section continued

Turnover Frequency

TOF values were calculated using following equations: TOF= (J×S)/(2×F×n) for HER, where, J is the current density (mA cm^{-2}) at specified overpotential, S is the surface area (cm^2) of the catalyst, F is the Faraday constant (96485.3 C mol^{-1}) and n is the number of moles of the active materials.

DFT Calculations

All the calculations were performed based on spin-polarized periodic density functional theory (DFT) implemented in Gaussian 09W. [1] The calculation basis set was B3LYP and the total energy convergence was set to be lower than 10^{-5} eV, and the force convergence was set to be smaller than 0.02 eV/Å. The potential of all the calculations were set to 0 V. The Gibbs free energy change (ΔG) of each reaction step is calculated as:

$$\Delta G = E_{tot(b)} - E_{tot(a)} + \Delta E_{ZPE} - T\Delta S$$

where $E_{tot(b)}$ is the energy of the given unit cell with intermediate of the latter state, $E_{tot(a)}$ is the energy of the intermediate of the previous state, ΔE_{ZPE} is the difference corresponding to the zero point energy change between the intermediates of the previous state and the latter state, ΔS is entropy change between the intermediates of the previous state and the latter state, and T represents the temperature applied for HER.

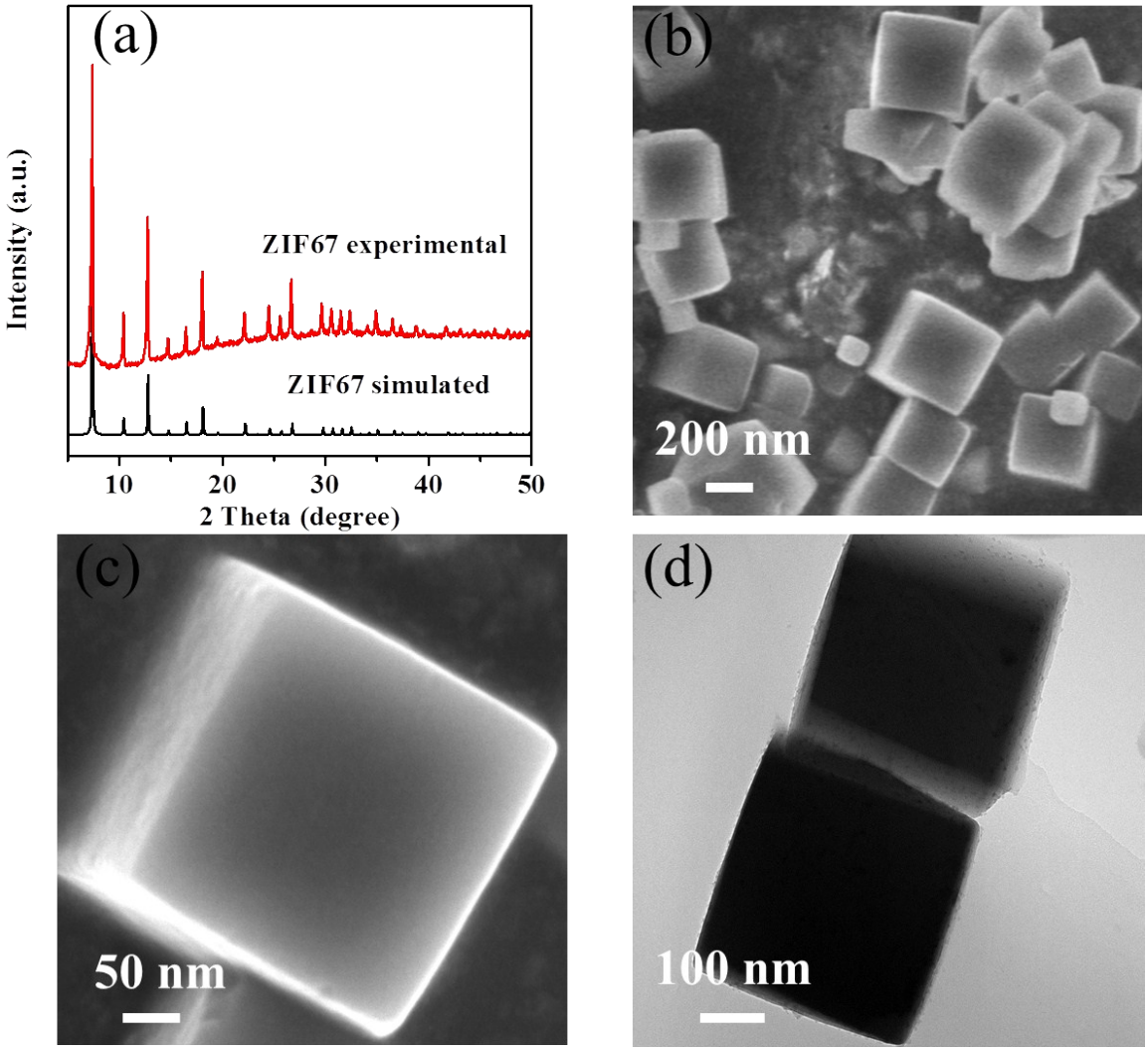

Figure S1. (a) XRD spectrum of ZIF67. (b and c) SEM images and (d) TEM image of ZIF67.

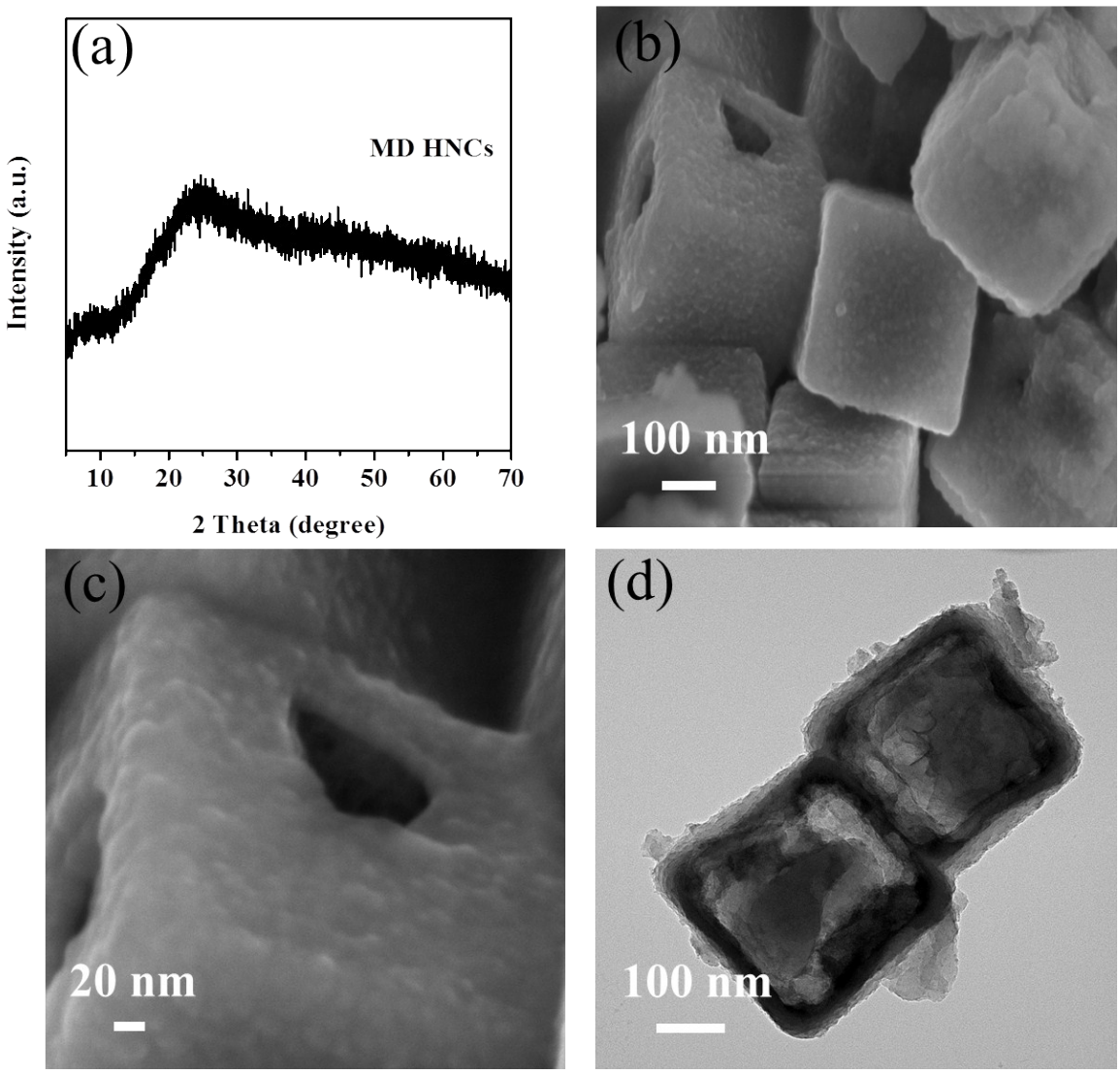

Figure S2. (a) XRD spectrum of MD HNCs. (b and c) SEM images and (d) TEM image of MD HNCs.

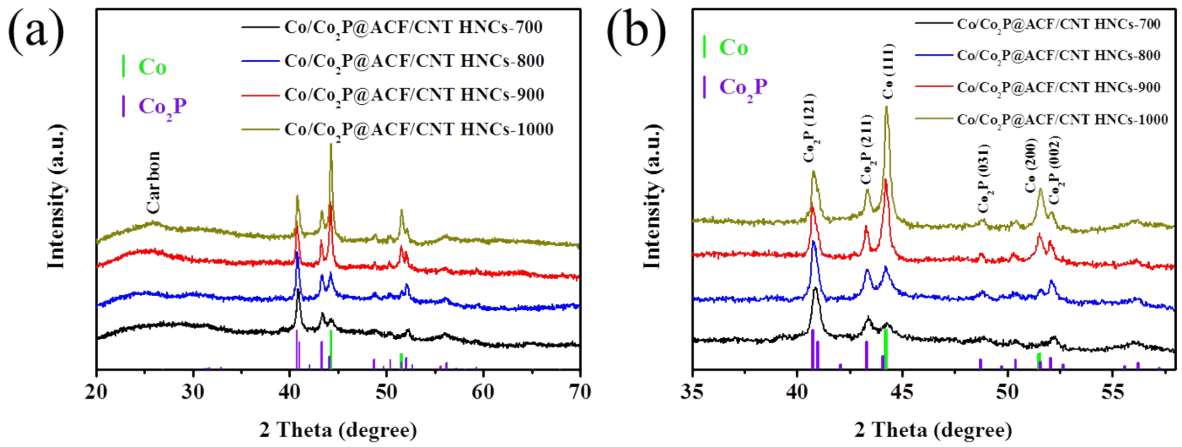

Figure S3. XRD spectra of Co/Co_2P@ACF/CNT HNCs annealed at different temperature.

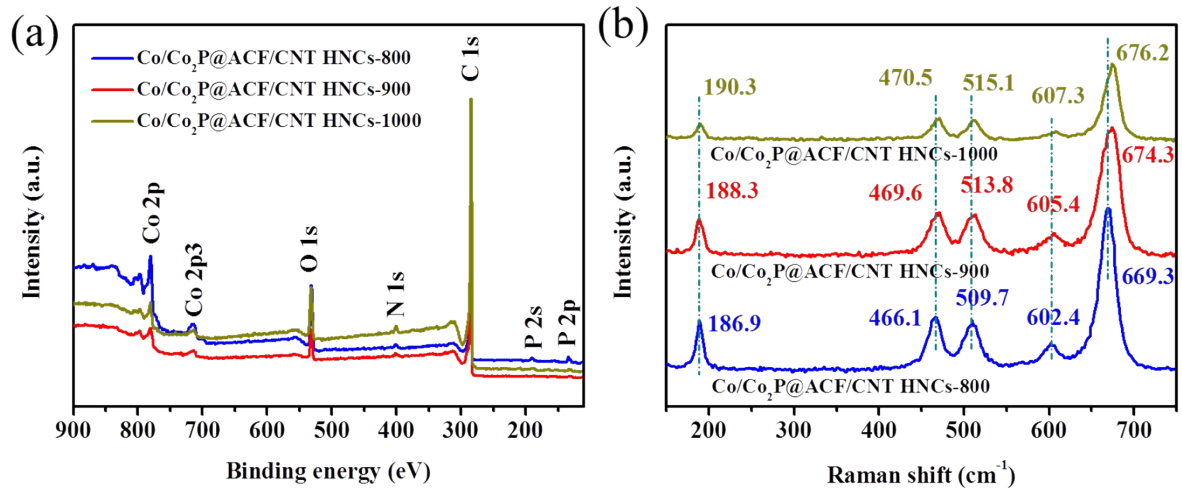

Figure S4. (a) XPS Survey spectra and (b) Raman spectra between 150 and 750 cm^{-1} showing the blue shift with the increasing the annealing temperature of Co/Co_2P@ACF/CNT HNCs-800, -900 and -1000 samples.

Table S1. Textural properties of the as-prepared Co/Co_2P@ACF/CNT HNCs catalysts.

Catalyst	BET surface area ($m^2\ g^{-1}$)	Pore volume ($cm^3\ g^{-1}$)
Co/Co_2P@ACF/CNT HNCs-800	211	0.043
Co/Co_2P@ACF/CNT HNCs-900	327	0.082
Co/Co_2P@ACF/CNT HNCs-1000	288	0.077

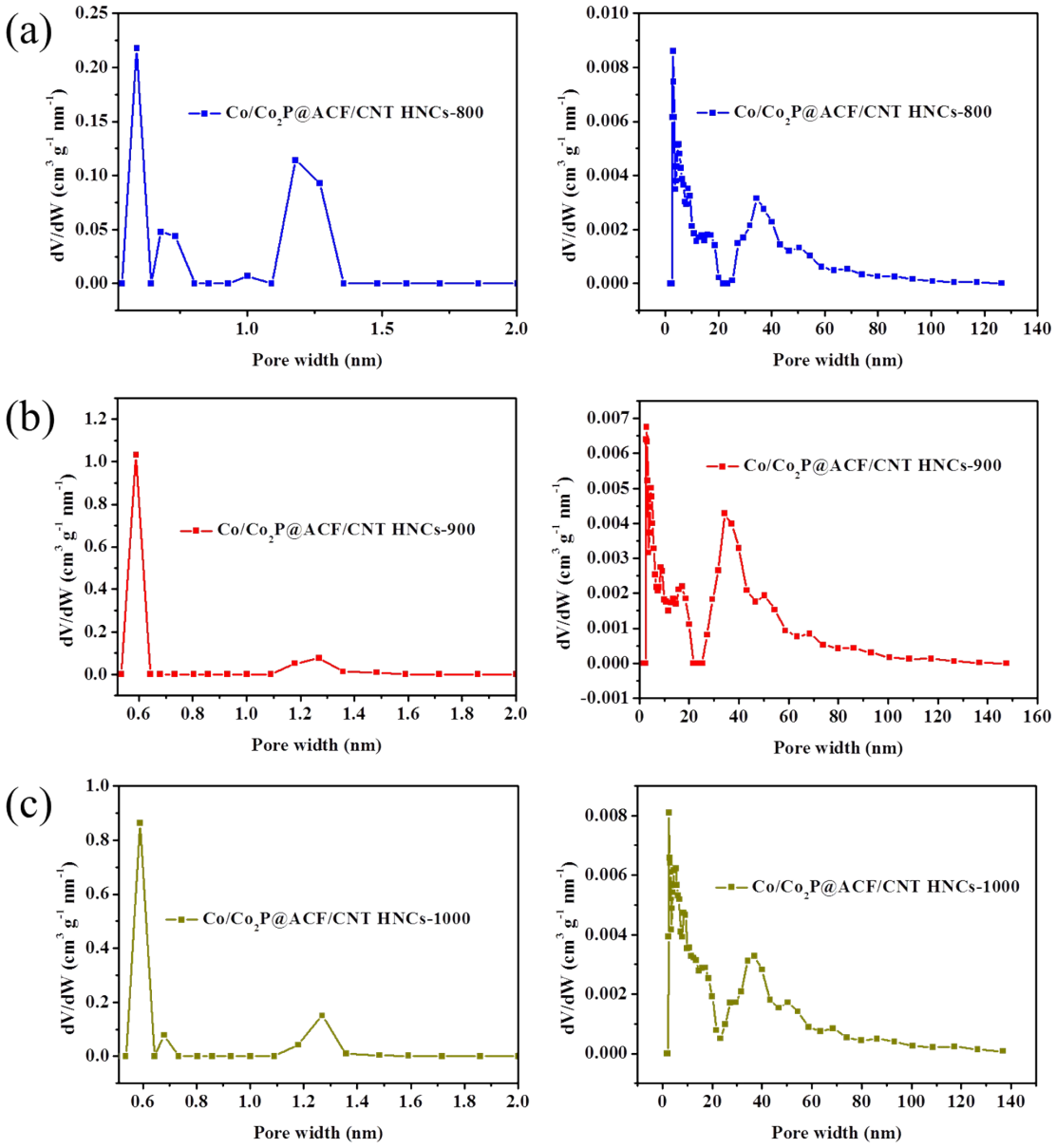

Figure S5. Pore size distribution of (a) Co/Co_2P@ACF/CNT HNCs-800, (b) Co/Co_2P@ACF/CNT HNCs-900 and (c) Co/Co_2P@ACF/CNT HNCs-1000.

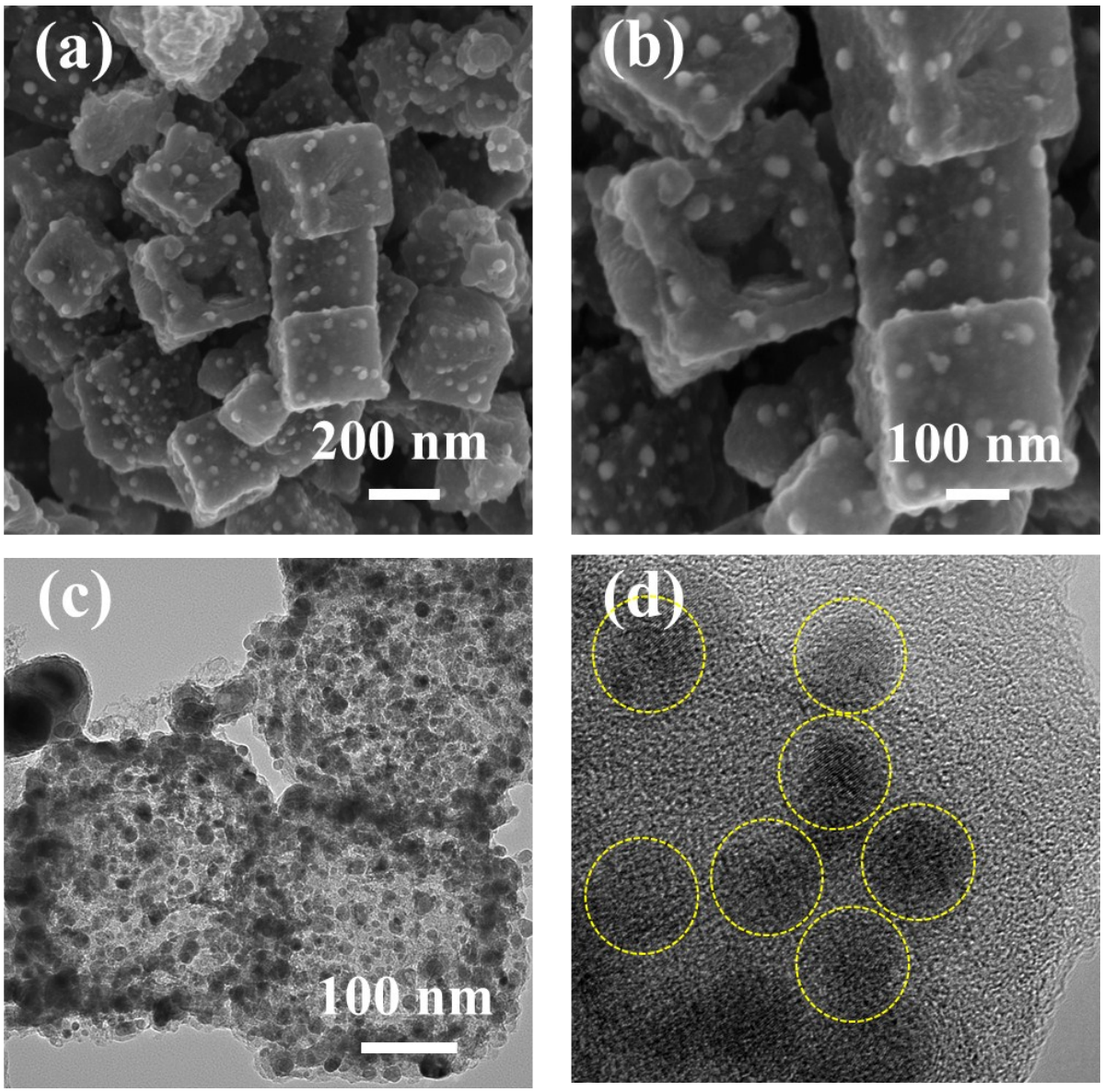

Figure S6. (a and b) SEM images of Co/Co_2P@ACF/CNT HNCs-800. (c and d) TEM images of Co/Co_2P@ACF/CNT HNCs-800.

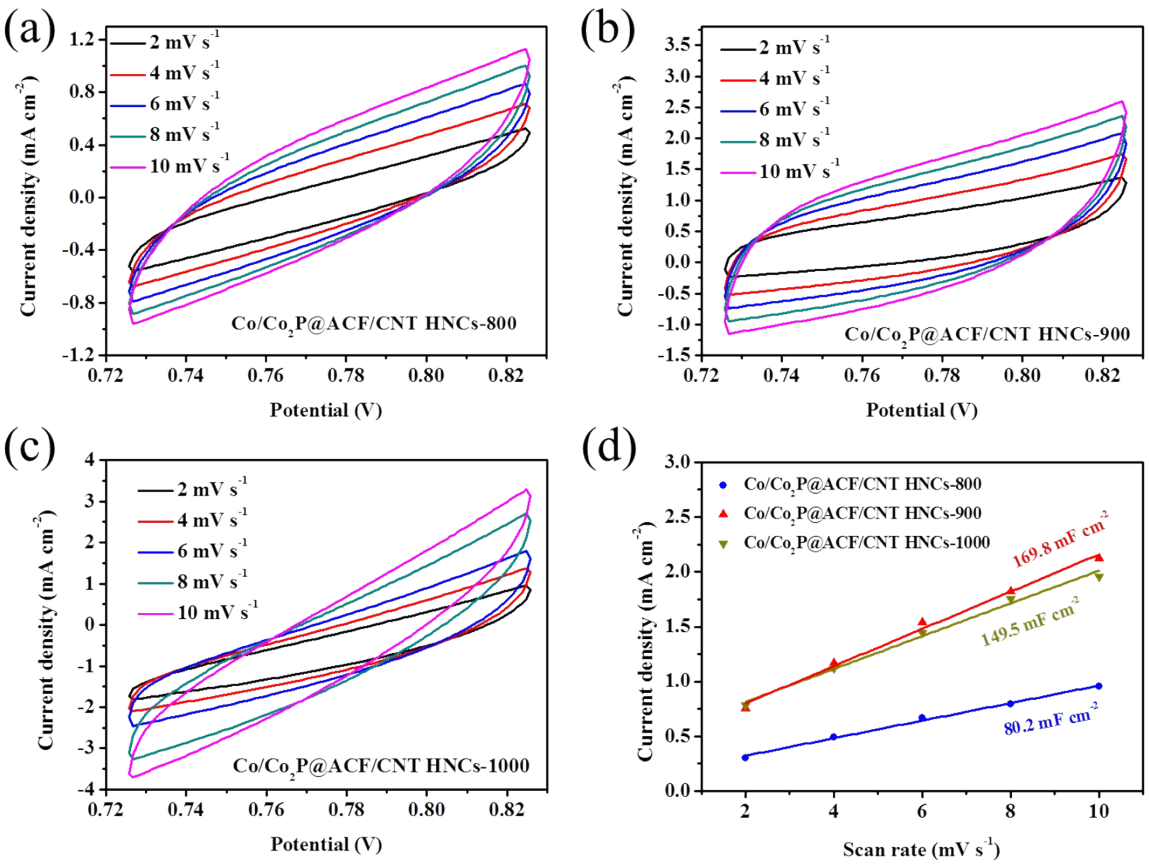

Figure S7. CV of (a) Co/Co_2P@ACF/CNT HNCs-800, (b) Co/Co_2P@ACF/CNT HNCs-900 and (c) Co/Co_2P@ACF/CNT HNCs-1000 in 1 M KOH solution in the region of 0.725-0.825 V vs. RHE for HER. (d) The differences in current density variation ($\Delta J=J_a-J_c$) of Co/Co_2P@ACF/CNT HNCs-800, -900 and -1000 electrocatalysts at an overpotential of 0.775 V plotted against the scan rate fitted to a linear regression enables the estimation of C_{dl}.

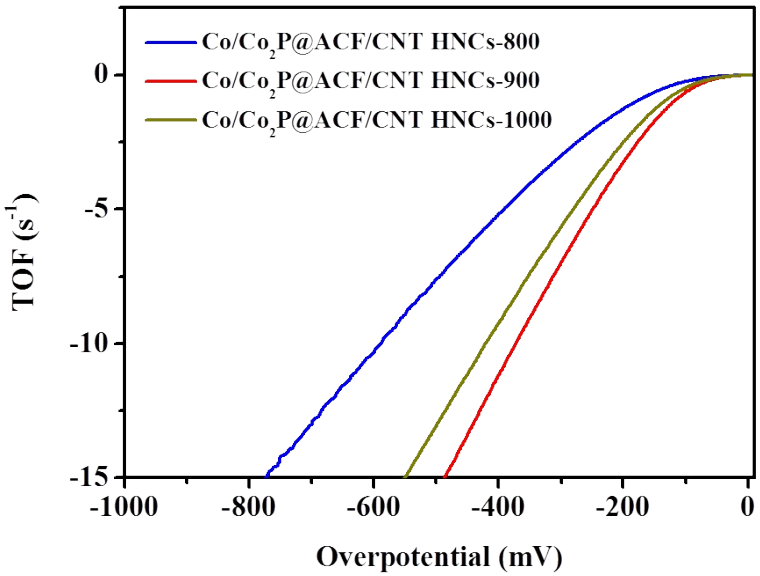

Figure S8. HER TOF plots of Co/Co_2P@ACF/CNT HNCs-800, -900 and -1000 samples.

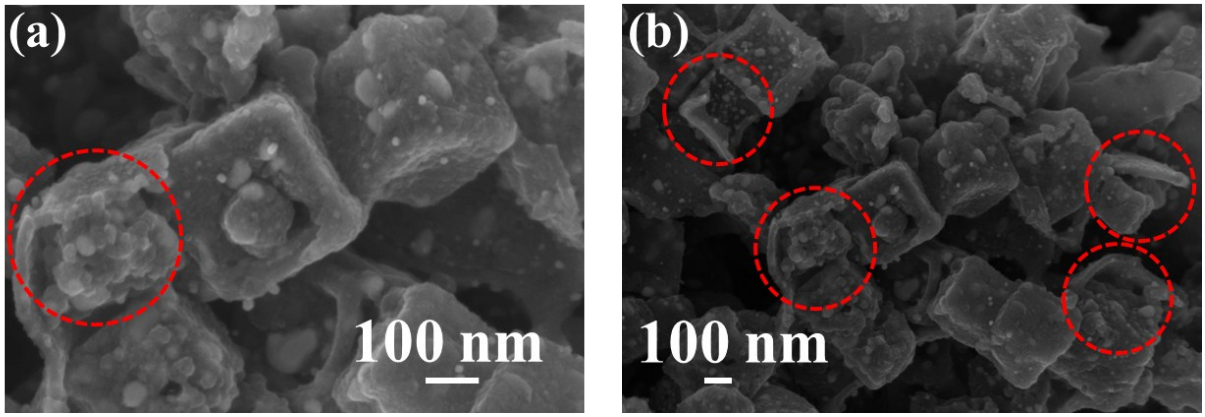

Figure S9. SEM images of Co/Co_2P@ACF/CNT HNCs-1000 sample showing damages in its morphology.

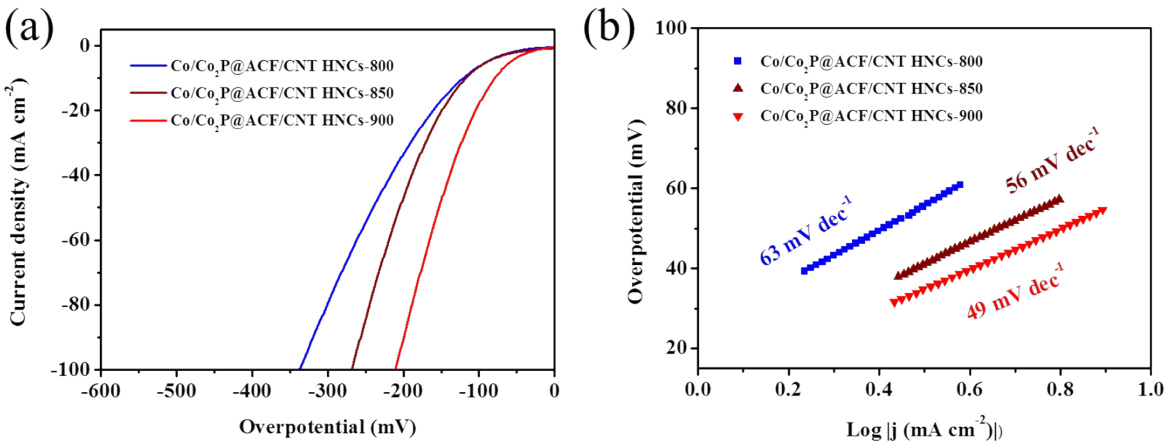

Figure S10. (a) LSV and (b) Tafel slope of Co/Co_2P@ACF/CNT HNCs annealed at different temperature.

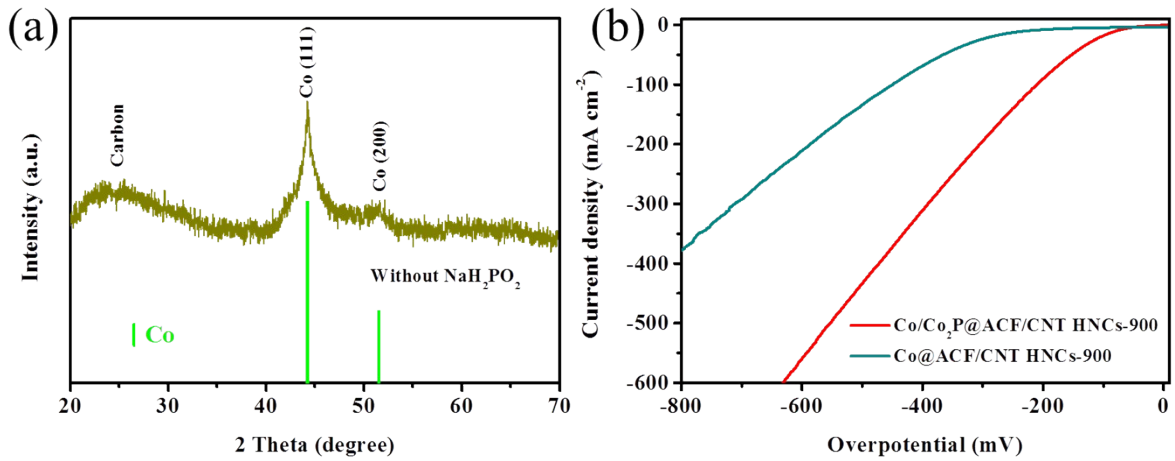

Figure S11. (a) XRD spectrum of Co@ACF/CNT HNCs-900. (b) LSV plots of Co/Co_2P@ACF/CNT HNCs-900 and Co@ACF/CNT HNCs-900.

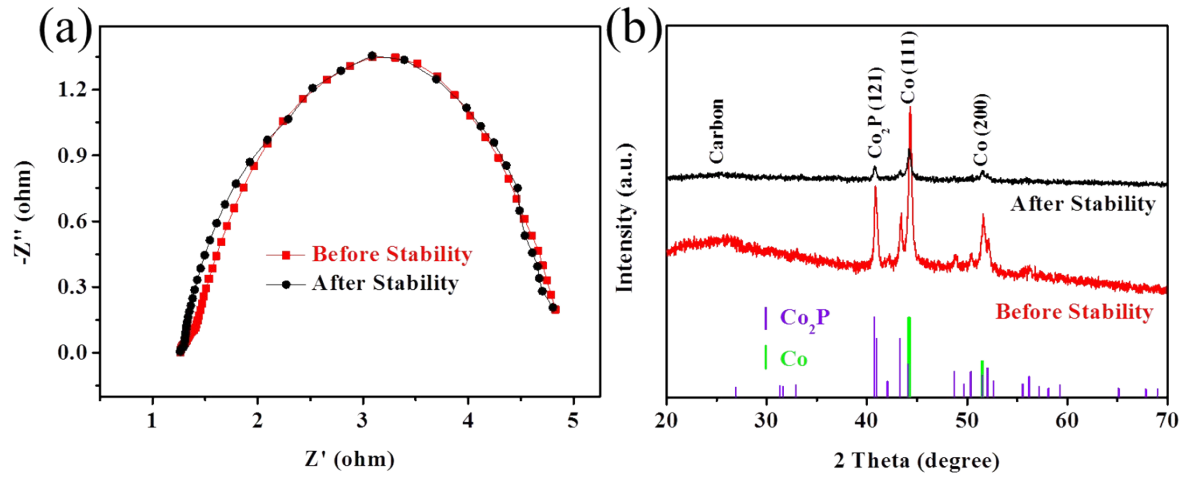

Figure S12. (a) Nyquist plots and (b) XRD spectra of Co/Co_2P@ACF/CNT HNCs-900 before and after stability test.

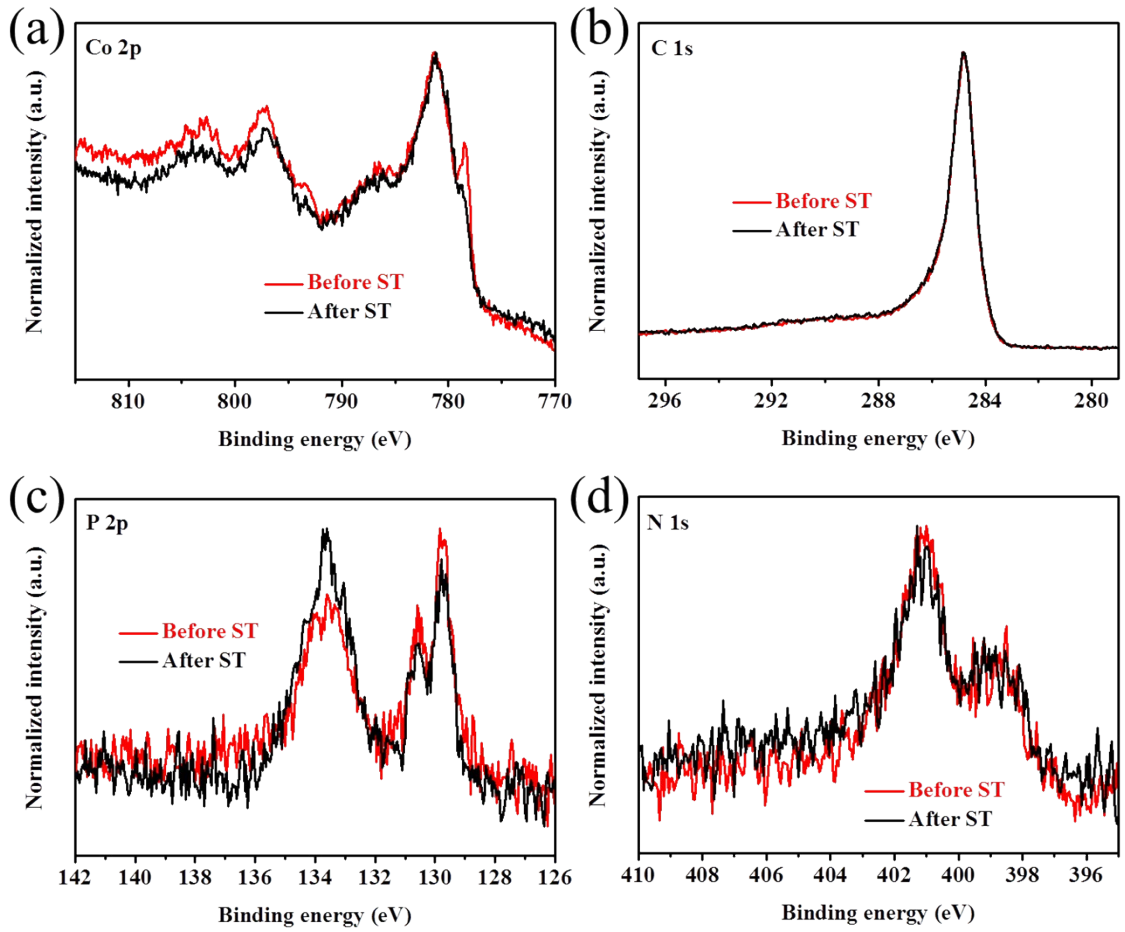

Figure S13. (a) Co 2p, (b) C 1s, (c) P 2p and (b) N 1s XPS spectra of Co/Co_2P@ACF/CNT HNCs-900 before and after stability test.

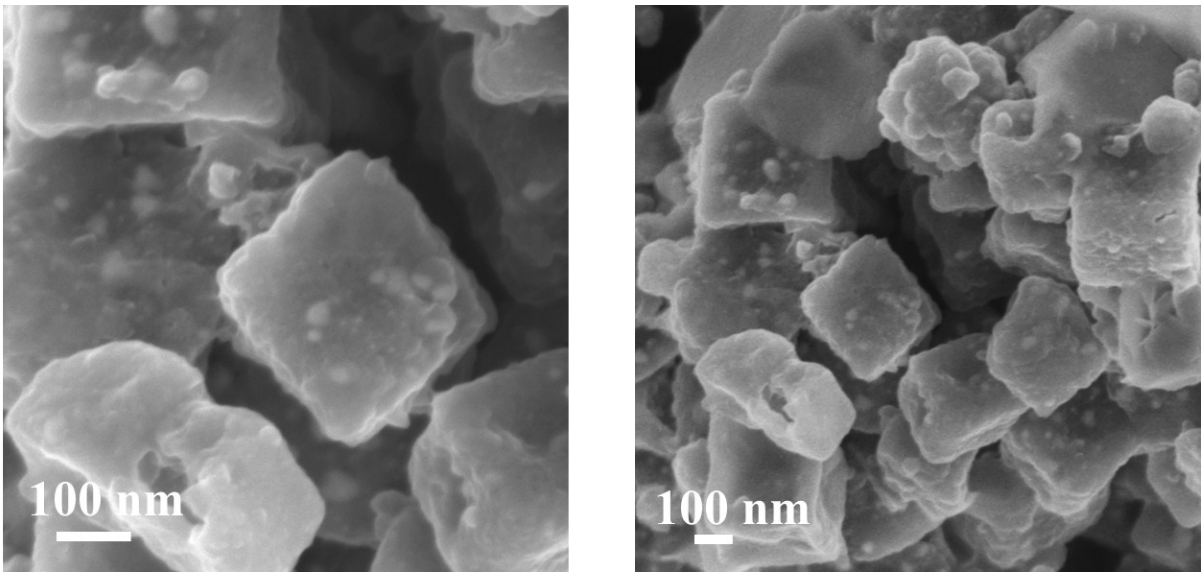

Figure S14. SEM images of Co/Co_2P@ACF/CNT HNCs-900 after stability test.

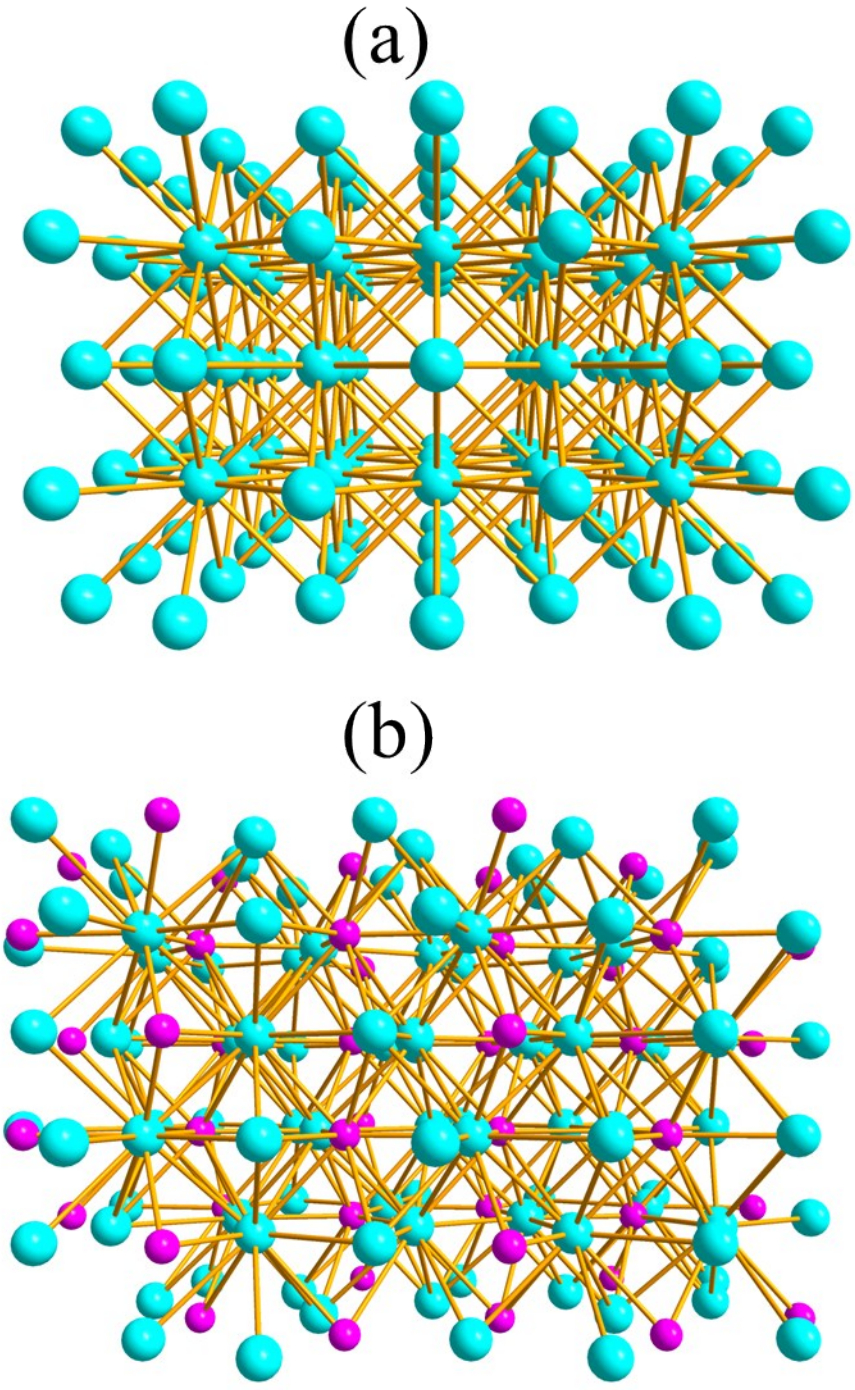

Figure S15. The optimized structures of (a) Co and (b) Co_2P.

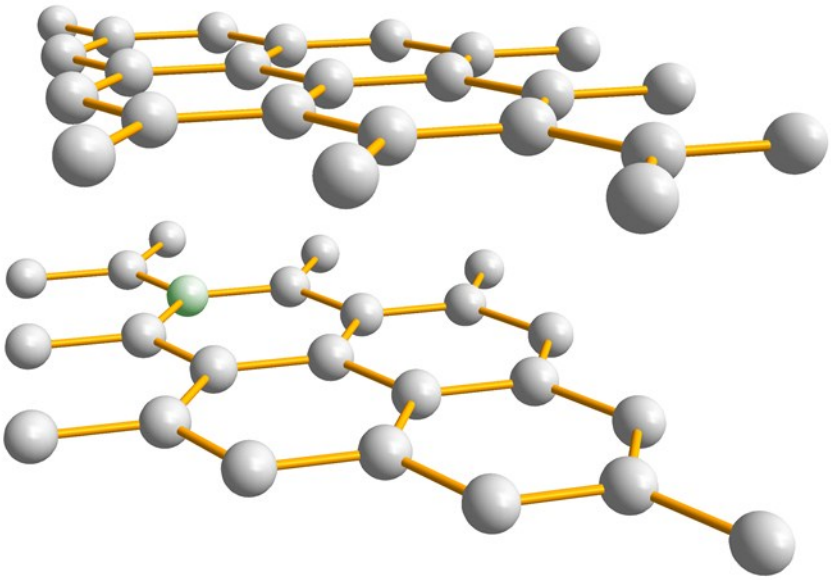

Figure S16. The optimized structures of graphitic amorphous carbon.

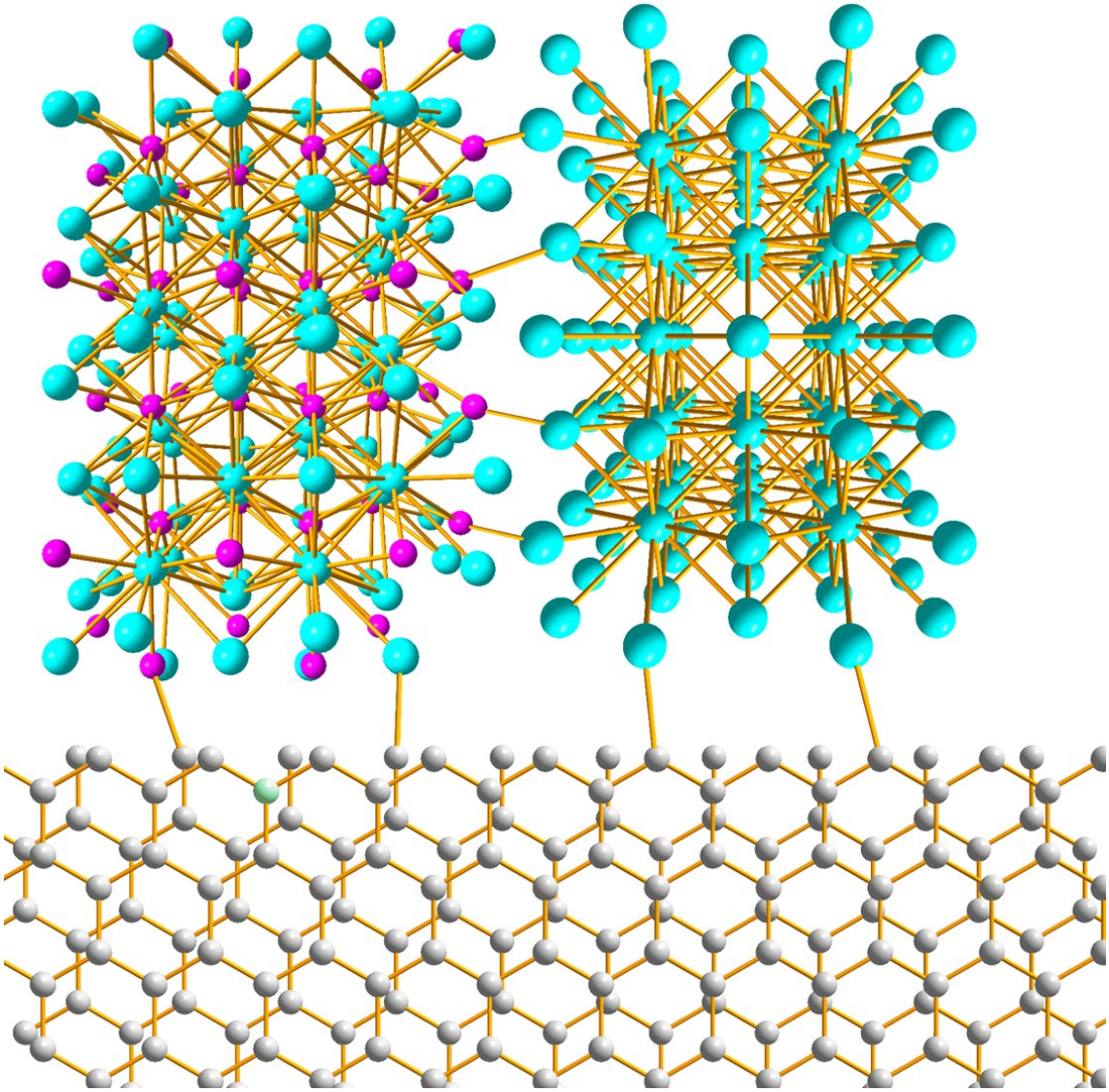

Figure S17. The optimized structures Co/Co_2P@ACF/CNT HNCs.

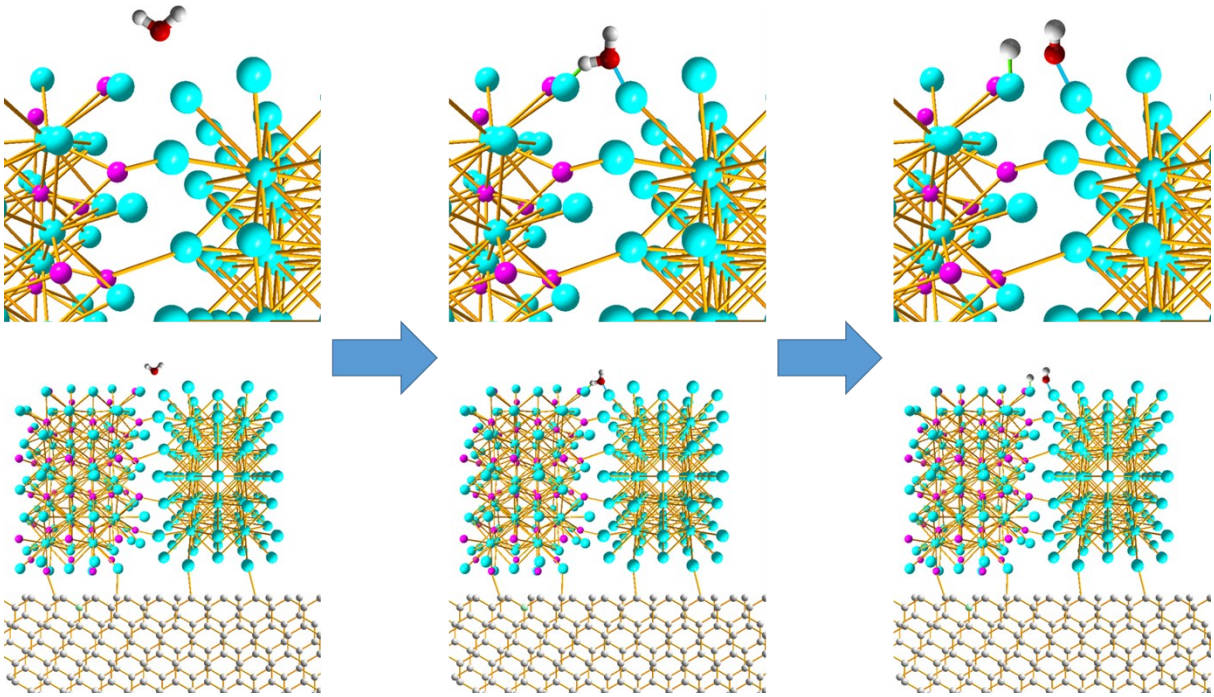

Figure S18. The optimized structures Co/Co_2P@ACF/CNT HNCs showing adsorption sites of H and H_2O.

Table S2. HER Performance comparison of our "*hybrid implanted hybrid*" electrocatalysts with MOF-derived Co-based catalysts.

Catalyst	η_{10} (mV)	Tafel slope (mV dec^{-1})	Stability
Co/Co_2P@ACF/CNT HNCs-900	78	49	48 h
Co/Co_2P@ACF/CNT HNCs-800	121	63	48 h
CoP/NCNHP [1]	115	66	20 h
$Cu_{0.3}Co_{2.7}P$/NC [2]	220	122	1000 cycles
CoP/rGO-400 [3]	150	38	22 h
Co4Ni1P NTs [4]	129	52	20 h
CoP@BCN [5]	215	52	8.5 h
$Co_{0.68}Fe_{0.32}P$ [6]	116	64	1 h
Co-P/NC [7]	191	51	1000 cycles
$Co_{5.47}N$ NP@N-PC [8]	149	86	10 h
Co-NC/CNT [9]	263	125	30000 s
$Co_{0.59}Fe_{0.41}P$ [10]	92	72	17 h
Ni-Co-P-300 [11]	150	60.6	1000 cycles
Co-Ni-P-300 [11]	167	71.2	-
Co-P-300 [11]	280	94.1	-
PNC/Co [12]	270	131	10 h
$CoSe_2$/CF [13]	95	50	20 h

References

1. Y. Pan, K. Sun, S. Liu, X. Cao, K. Wu, W.-C. Cheong, Z. Chen, Y. Wang, Y. Li, Y. Liu, D. Wang, Q. Peng, C. Chen and Y. Li, *J. Am. Chem. Soc.*, 2018, **140**, 2610-2618.

2. J. Song, C. Zhu, B. Z. Xu, S. Fu, M. H. Engelhard, R. Ye, D. Du, S. P. Beckman and Y. Lin, *Adv. Energy Mater.*, 2017, **7**, 1601555.

3. L. Jiao, Y.-X. Zhou and H.-L. Jiang, *Chem. Sci.*, 2016, **7**, 1690-1695.

4. L. Yan, L. Cao, P. Dai, X. Gu, D. Liu, L. Li, Y. Wang and X. Zhao, *Adv. Funct. Mater.*, 2017, **27**, 1703455.

5. H. Tabassum, W. Guo, W. Meng, A. Mahmood, R. Zhao, Q. Wang and R. Zou, *Adv. Energy Mater.*, 2017, **7**, 1601671.

6. F. Li, Y. Bu, Z. Lv, J. Mahmood, G.-F. Han, I. Ahmad, G. Kim, Q. Zhong and J.-B. Baek, *Small*, 2017, **13**, 1701167.

7. B. You, N. Jiang, M. Sheng, S. Gul, J. Yano and Y. Sun, *Chem. Mater.*, 2015, **27**, 7636-7642.

8. Z. Chen, Y. Ha, Y. Liu, H. Wang, H. Yang, H. Xu, Y. Li and R. Wu, *ACS Appl. Mater. Interfaces*, 2018, **10**, 7134-7144.

9. F. Yang, P. Zhao, X. Hua, W. Luo, G. Cheng, W. Xing and S. Chen, *J. Mater. Chem. A*, 2016, **4**, 16057-16063.

10. J. Hao, W. Yang, Z. Zhang and J. Tang, *Nanoscale*, 2015, **7**, 11055-11062.

11. Y. Feng, X.-Y. Yu and U. Paik, *Chem. Commun.*, 2016, **52**, 1633-1636.

12. X. Li, Z. Niu, J. Jiang and L. Ai, *J. Mater. Chem. A*, 2016, **4**, 3204-3209.

13. C. Sun, Q. Dong, J. Yang, Z. Dai, J. Lin, P. Chen, W. Huang and X. Dong, *Nano Res.*, 2016, **9**, 2234-2243.